Chemical Engineering Science 260 (2022) 117842

Contents lists available at ScienceDirect

Chemical Engineering Science

journal homepage: www.elsevier.com/locate/ces

Hydrodynamics in a three-phase flotation system – Fluid following with a new hydrogel tracer for Positron Emission Particle Tracking (PEPT)

Diego Mesa [a,*], Michael van Heerden [b,c,*], Katie Cole [b], Stephen J. Neethling [a], Pablo R. Brito-Parada [a]

[a] Advanced Mineral Processing Research Group, Royal School of Mines, Imperial College London, United Kingdom
[b] Department of Physics, University of Cape Town, South Africa
[c] iThemba LABS, Cape Town, South Africa

HIGHLIGHTS

- A new neutrally-buoyant hydrogel tracer for PEPT was tested in a flotation system.
- This new hydrogel tracer can withstand the shear rate of a stirred tank's impeller.
- The hydrogel tracer has different residence times and velocities than resin tracers.
- Fast ascending liquid flows were observed near the walls of the tank.

GRAPHICAL ABSTRACT

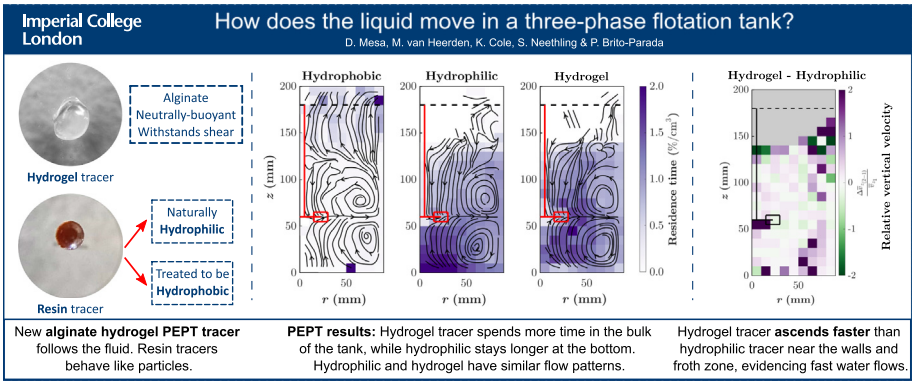

ARTICLE INFO

Article history:
Received 24 January 2022
Received in revised form 7 June 2022
Accepted 28 June 2022
Available online 30 June 2022

Keywords:
Froth flotation
Hydrodynamics
PEPT
Alginate hydrogel tracer
Neutrally-buoyant tracer

ABSTRACT

Understanding the hydrodynamics of three-phase stirred tanks, such as froth flotation cells, is paramount for the characterisation of turbulence, stability and performance. Although positron emission particle tracking (PEPT) is known for its effectiveness in measuring the hydrodynamics of particles in opaque, high solid content systems, it has not been widely used for characterising the liquid phase. This work presents a new, neutrally buoyant, alginate hydrogel tracer, designed to emulate the density of the liquid phase, which is suitable for high-speed tracking with PEPT.

PEPT experiments were conducted in a bench-scale flotation cell, comparing the new tracer to ion-exchange resin tracers previously used in this system. Results showed statistically significant differences in pathlines, residence time and velocity distribution among the tracers. Moreover, the hydrodynamics of the new tracer agree with existing CFD predictions for the liquid phase. This methodology enables the comprehensive study of relative flow behaviour in complex multiphase systems.

1. Introduction

Aerated stirred tanks are widely used reactors in several industrial processes (Kumaresan and Joshi, 2006; Yang and Mao, 2014), where two or three phases (air, liquid, and solids) are mixed by the action of an impeller. The hydrodynamics of the different phases can have a major effect on the performance of the processes (*e.g.*

* Corresponding authors at: Imperial College and Michael van Heerden at University of Cape Town (D. Mesa). Department of Physics, University of Cape Town, South Africa (M. van Heerden).

E-mail addresses: d.mesa@imperial.ac.uk (D. Mesa), michael.vanheerden@uct.ac.za (M. van Heerden).

https://doi.org/10.1016/j.ces.2022.117842
0009-2509/

de Lamotte et al., 2017; Rosseburg et al., 2018; Deglon, 2005; Tabosa et al., 2016). Several experimental techniques have thus been developed to characterise the hydrodynamics of each phase. A review of these different experimental techniques can be found in Mavros (2001) and Ascanio (2015).

The term "gas hydrodynamics" has been commonly used for the study of gas dispersion in terms of gas holdup (Maximiano Raimundo et al., 2019; Gomez and Finch, 2007; Liu et al., 2011) and bubble size distribution(Alves et al., 2002; Martín et al., 2008; Montante et al., 2008; Gomez and Finch, 2007; Grau and Heiskanen, 2002), which have been well characterised for two- and three-phase experimental setups on average terms. However, there are fewer studies that have assessed the dynamic, instantaneous behaviour and spatial distribution of the gas phase. Techniques such as electrical resistance tomography (Wang et al., 2000; Montante and Paglianti, 2015; Hashemi et al., 2016), γ-ray/X-ray tomography (Hampel et al., 2007; Boden et al., 2008; Ford et al., 2008) and multiple probes for image analysis (Xiao et al., 2020) have been implemented to measure the spatial distribution of gas holdup with time, but there is still limited data on the gas velocity distribution within opaque stirred systems.

The hydrodynamics of the liquid phase in stirred tanks has been extensively studied using optical techniques, such as laser Doppler velocimetry (LDV) (Armenante et al., 1997; Mavros et al., 2002; Schwarz et al., 2019) and particle image velocimetry (PIV) (Brady et al., 2006; de Lamotte et al., 2018; Sommer et al., 2021). However, these techniques can only be applied in transparent or translucent systems, or without solid particles entirely. Schubert (2008) showed that the presence of suspended particles considerably diminishes the turbulence intensity in fluid systems. Consequently, the hydrodynamics of the liquid-phase in three-phase opaque systems cannot be accurately studied using simplified translucent systems, and appropriate techniques for opaque systems are required.

Positron emission particle tracking (PEPT) has been successfully applied to assess the hydrodynamics of the solid phase in different opaque systems, from dish-washing machines (Pérez-Mohedano et al., 2015) and spouted bed roasters (Al-Shemmeri et al., 2021) to milling equipment (Yu et al., 2015) and froth flotation tanks (Waters et al., 2008; Mesa et al., 2021; Cole et al., 2022b). PEPT is a non-invasive technique that can be used to track the position of a particle within a vessel over time. This technique measures penetrating radiation and is not based on optical properties, thus making it suitable for opaque and dense systems such as flotation tanks. In PEPT experiments, a radiolabelled tracer particle is tracked using a Positron Emission Tomography (PET) camera (Parker et al., 1993). The positron emitted by the tracer tends to annihilate with an electron from local matter which produces a pair of almost back-to-back gamma rays ($180^\circ \pm 0.5^\circ$) (Spinks et al., 2000). If the PET camera detects both gamma rays from the pair in coincidence, within a short time window of approximately 7 ns, the annihilation event can be located somewhere along the path between the two detectors. This location event forms a line of response (LoR), and with multiple LoRs the location of a moving tracer particle can be triangulated with time (Parker et al., 1993). The measurement produces time series data on the tracer location, which can be used to determine the tracer velocity and time averaged analyses such as the hydrodynamics. The tracers used in PEPT are either representative particles that work as proxies of the real particles of interest – often indirectly activated Fan et al. (2006, 2014) – or identical to the particles studied – often directly activated (for more information on tracer activation, the reader is referred to Boucher et al., 2017; Fan et al., 2006).

Although PEPT has been extensively used for determining the hydrodynamics of solid particles in opaque systems, there are fewer applications in the literature using PEPT to study the dynamics of the liquid phase. This is particularly the case for three-phase systems. Earlier work focused on achieving flow following behaviour by controlling the density of the tracer to obtain neutral buoyancy or be isokinetic with the fluid flow, such as tracking viscous fluids and impeller designs Fangary et al. (2000),Bakalis et al. (2004), Chiti et al. (2011). In more recent times, researchers from the University of Tennessee-Knoxville have renewed interest in using tracer particles as fluid followers in systems of flow Langford et al. (2016),Wiggins et al. (2019).

Pianko-Oprych et al. (2009) modified the density of the liquid in their single-phase mixing system so that a tracer particle fabricated from an ion exchange resin was neutrally-buoyant. Upwards and downwards pumping motions in turbulent flow were investigated with a pitched blade turbine (PBTU and PBTD, respectively), by measuring the hydrodynamics of the resin particle. It is likely that the system was actually two-phase, in comparison to being reported as single-phase, because the impeller speed was high enough for substantial air to be suctioned from the free surface. The behaviour of the neutrally-buoyant tracer (diameter 600 μm) was compared with that of a directly activated single glass-particle tracer (diameter 2.85–3.3 mm) in a 5 wt% two-phase solid–liquid system (again, with substantial entrainment of air from the free surface). The results suggested that the liquid and solid phases moved at similar speeds but that, on average, the denser, glass particle ascended more slowly than the neutrally-buoyant resin tracer with the PBTU configuration, whereas the glass particle descended more quickly with the PBTD configuration. The difference between the tracers suggests the resin particle acted as a proxy for the liquid phase. However, the impact of this comparison is limited by the differences between the systems used to test the tracers, and the differences in size of the tracers.

Specifically for the context of using hydrogels for PEPT tracers, Fairhurst et al. (2001) used almost spherical alginate particles that were neutrally-buoyant, with a specific gravity of 1.02. The tracer, a 600μm diameter resin bead radiolabelled with the positron-emitting radionuclide ^{18}F, was placed inside one of the alginate particles, with final size 5–10 mm. This method enabled the characterisation of the liquid flow patterns in a pipe, for a system with high solids content (20% to 40% v/v). However, the particle size used for tracking was large, limiting their application to flow applications with length scales larger than the tracer size. Moreover, the work studied flow in a pipe, whereas for stirred tanks the tracer must be shown to withstand high turbulence conditions created by an impeller.

In this work, a new hydrogel tracer particle is used for PEPT measurements; fabricated from alginates to produce a neutrally-buoyant particle. The behaviour of the hydrogel tracer is compared to that of two solid-particle tracers – a hydrophobic and a hydrophilic tracer – of similar size and activity in a three-phase 20 wt % flotation system agitated with a Rushton turbine.

The experimental system selected for testing the tracers was froth flotation, as its complexity enables the characterisation of the tracers' behaviour under highly different turbulent regimes in an opaque three-phase system. Froth flotation is the most important mineral separation process because of its technical versatility and cost-effectiveness (Wills and Finch, 2016; Mesa and Brito-Parada, 2019). In a mechanical flotation cell, particles with different surface properties are suspended in a highly turbulent aerated slurry. The hydrophobic particles attach to the small bubbles dispersed in the system and rise due to buoyancy, forming a quiescent particle-laden froth that overflows as concentrate (Wills and Finch, 2016).

Flotation is widely used not only in mineral processing but also in oil sands concentration (Rao and Liu, 2013), ionic flotation (Polat and Erdogan, 2007), algae separation (Laamanen et al., 2016), paper deinking (Vashisth et al., 2011), plastic recycling (Wang

et al., 2015; Negari et al., 2018), water treatment (Saththasivam et al., 2016) and lithium-ion batteries recycling (Zhang et al., 2018, 2020, 2018, 2020). The study of its complex hydrodynamics, therefore, is an important challenge that can result in improved designs, more efficient operations and a better understanding of the flow phenomena.

2. Experimental

2.1. Aerated stirred tank design and operation

All the experiments were performed using a 4-litre aerated stirred tank formed of acrylic Norori-McCormac et al. (2017),Mesa et al. (2021). The geometry of the flotation tank, as shown in Fig. 1, followed the design of a standard mixing tank (Rushton et al., 1950; Eckert et al., 1985). The tank was fitted with a Rushton turbine to agitate the three-phase suspension. Air was diffused into the tank through a frit with a mesh hole-size of 20 μm, to produce small bubbles.

The tank was operated continuously by recirculating the overflowing froth to achieve steady state. Operating at steady state allows for the behaviour of the system to be representative of that of industrial flotation cells. This continuous operation in a closed-loop is also required for PEPT measurements as it makes it possible to run experiments for longer periods of time to acquire an adequate amount of data, since the radio-labelled tracer is always returned to the tank in the case it overflows into the concentrate launder (Cole et al., 2022a).

2.2. Materials and reagents

Glass beads with a particle size ranging between 75 μm and 150 μm were used as the solids in the system. The beads were sourced from Blastrite Ltd (Cape Town). The composition of the glass beads was the same as detailed in Mesa et al. (2020). Deionised water was used to prepare 3.3 litres of pulp at 20% solid content by weight. This single-species system has been used before due to its simplicity (Mesa et al., 2020; Norori-McCormac et al., 2017).

Dowfroth 250 (DF250, provided by Nasaco) was used as a frother, added at an initial dose of 4.0 μl per litre of water (4.0 ppm in volume), with an additional dose of 0.4 ppm every 30 min. The collector used was Tetradecyltrimethylammonium bromide (TTAB, Sigma Aldrich), added at an initial dose of 4.0 g/t and continuous addition at a rate of 2.0 g/(t h).

2.3. PEPT tracers

Three different tracers were used in this work - hydrophobic and hydrophilic resin beads, and an alginate hydrogel. The first two resin bead tracers have been previously and described in the literature (Cole et al., 2014; Mesa et al., 2021; Cole et al., 2022b) for the characterisation of the hydrodynamics of particles. The hydrophobic and hydrophilic tracers represent valuable and non-valuable flotation minerals, respectively. The third tracer corresponds to a new, neutrally-buoyant hydrogel tracer that represents the hydrodynamic behaviour of the liquid phase.

The core of the hydrophobic and hydrophilic tracers was prepared using Purolite NRW100 cation exchange resin beads labelled with ^{68}Ga with a half-life of 68 min, as described in Cole et al. (2014, 2021). The ^{68}Ga used for producing tracers was eluted from a 30 mCi SnO_2 based ^{68}Ge/^{68}Ga generator (supplied by iThemba LABS, South Africa) using diluted hydrochloric acid. The ^{68}Ga solution was evaporated to incipient dryness before being re-dissolved in deionised water to reduce the acidity of the solution. A maximum of three NRW-100 cation exchange resin beads were selected based on visual inspection for flaws and appropriate size before being added to a small glass vial. Size measurements were also made by comparison against a calibrated eye-piece mounted within an inverted microscope.

The cores were then coated to manipulate the physical properties to match the material of interest, *i.e.* generate hydrophobic and hydrophilic tracers. A rapid-set two-part epoxy was used to seal and manipulate both the hydrophobic and hydrophilic particles used in the study. The hydrophilic coating was made by exploiting the natural hydrophilic property of the epoxy resin and seal the selected resin bead. The hydrophobic tracer coating used the same epoxy resin as the hydrophilic tracer with the addition of a layer of silanized ballotini. The hydrophilic tracer had a final diameter of 440 ± 10 μm after being coated, while the hydrophobic coated tracer size was 550 ± 10 μm. The activities of the resin bead tracers were 690 ± 100 μCi and 1250 ± 100 μCi, respectively.

The hydrogel tracer production makes use of a purified ^{68}Ga solution described in detail by van Heerden et al. (2020), supplied by the same SnO_2 ^{68}Ge/^{68}Ga generator used for the production of the NRW-100 tracers. The ^{68}Ga is evaporated before being re-dissolved in an alginate solution that is then converted into a gel and finally sealed using a concentrated $CaCl_2$ salt solution to increase the survivability of the hydrogel tracer. This novel tech-

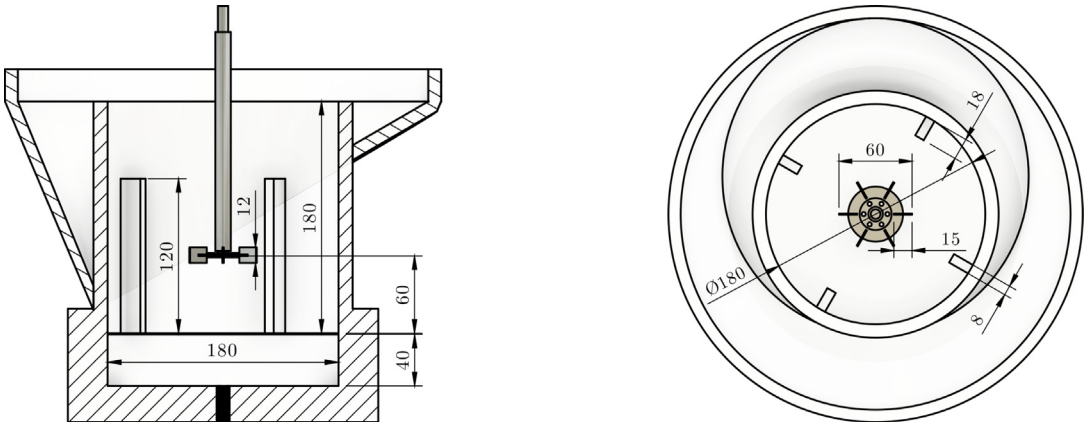

(a) Side (b) Top

Fig. 1. Aerated stirred tank, showing the dimensions in millimetres from a (a) lateral view and a (b) view from the top. The tank is fitted with a Rushton turbine and its proportions follow that of a standard mixed tank.

nique for producing ^{68}Ga hydrogel tracers is thoroughly described in Heerden et al. (2022).

The final hydrogel tracer had a size range 1.0 ± 0.1 mm (based on measurement of the particle width in a microscope image) and an activity of 1200 ± 100 μCi. An example of the final hydrogel particle is shown in Fig. 2, in comparison to an NRW-100 resin particle.

It is important to note that the tracers used were larger than the average particle size of a typical flotation feed. Since the radiolabelling efficiency ion exchange process is related to the surface area of the resin, there is a trade-off between the tracer having a representative size for flotation and having a high enough activity to enable high speed measurements (Cole et al., 2014; Mesa et al., 2021). In this work, the detection of high speeds, with high temporal and spatial resolution, has been prioritised over tracer size. The main limitation of using larger tracers is the inability to observe small-scale eddies and other turbulent structures of the flow smaller than the tracer size.

2.4. PEPT methodology

PEPT experiments were performed for each type of tracer - *i.e.* hydrophobic, hydrophilic and hydrogel - to study the hydrodynamics of the different phases of the system. The PEPT experiments were conducted at the PEPT Cape Town facility, situated within the iThemba LABS (South Africa). The PET camera used was a Siemens EXACT HR++ (schematic in Fig. 3), which is known for its high efficiency and large field of view (Buffler et al., 2018). The Siemens EXACT HR++ camera consists of 48 rings of standard bismuth germanate (BGO) detector elements (each 4.39 mm trans-axial $\times$ 4.05 mm axial $\times$ 30 mm deep, grouped in blocks of 8×8) with a ring diameter of 82 cm, producing an axial field of view of 23.4 cm (Buffler et al., 2018). This is significantly larger than other 'standard' ring geometry PET cameras. The data acquisition system can maintain a sustained acquisition rate of about 4 million coincidence events per second. The mean spatial resolution of the scanner for PET imaging has been measured to be 4.8 ± 0.2 mm FWHM (trans-axial, 1 cm off-axis) and 5.6 ± 0.5 mm (axial, on-axis) (Spinks et al., 2000).

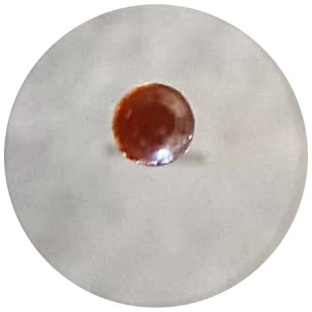

(a) NRW-100 resin tracer

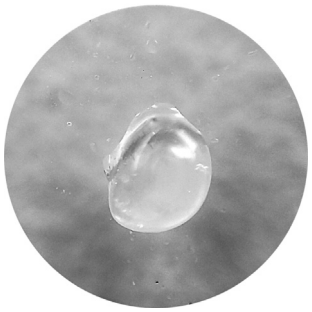

(b) Alginate hydrogel tracer

Fig. 2. PEPT tracers used in this work. The (a) NRW-100 resin bead tracer is used to represent the behaviour of the mineral particles, being coated with silanised ballotini to represent hydrophobic particles (to be floated) and with an epoxy resin to represent hydrophilic particles (not floated). The (b) hydrogel tracer is used to represent the behaviour of the water.

(a)

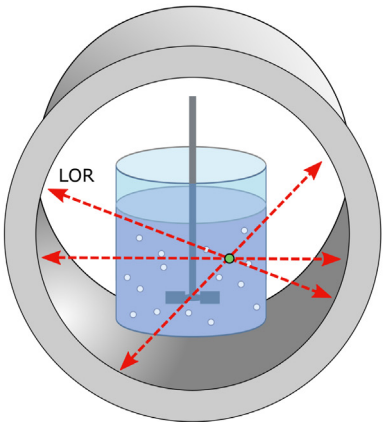

(b)

Fig. 3. Positron emission camera (a) photography, showing the flotation cell inside the HR++ PET camera at PEPT Cape Town, and (b) a schematic representation of the location process. The red lines represent the lines of response (LOR's) between pairs of opposite detectors in the ring.

Operating conditions were kept constant for all the experiments. The superficial gas velocity was set at 0.98 cm/s (equivalent to an air flow rate of 15 lpm), as it was found to be the optimum J_g in previous studies using this flotation cell and similar systems (Norori-McCormac et al., 2017; Mackay et al., 2020). The impeller speed was 1200 RPM, which achieved the same impeller tip speed (3.77 m/s) as the systems studied in Mesa and Brito-Parada (2020), Mesa et al. (2020),Mesa et al. (2021),Cole et al. (2022b). Froth depth was maintained at approximately 4 cm for all experiments, as the volume of pulp within the tank was constant throughout the flotation tests.

The experimental procedure for PEPT measurements in the flotation system is detailed in Mesa et al. (2021) and Cole et al. (2022a). Before each experiment, a location marker was positioned on the exterior wall of the flotation cell, to define the cell position within the PET camera field of view. The location marker was a small Perspex cylinder of 10 mm diameter encapsulating 13 μCi of ^{22}Na at its centre. Five different locations were tracked on the wall of the cell at the same height, producing a ring of known locations that aided in the alignment of the PEPT data within the

geometry of the flotation cell. To ensure sufficient data for time averaged analysis throughout the whole cell, each experiment was run for approximately 2 h.

The PEPT data analysis is thoroughly described in Mesa et al. (2021),Cole et al. (2022b) and Cole et al. (2022a). A summary description of the process is given next and in Fig. 4. The PEPT data were analysed using the location algorithm proposed by Parker et al. (1993) to determine the position of the tracer for each of the positron–electron annihilation events with time. In this algorithm, a number N of LORs are grouped while a closest passing fraction f of them are found by iteration, rejecting the rest of the data. These parameters were selected to minimise the noise/scatter around a potential track, using triangulation optimisation techniques, such as a rotating disc study (Parker et al., 1993; Mesa et al., 2021).

The triangulated data were smoothed using a cubic spline kernel with a half breadth of 4 ms for the pulp and of 12 ms for the froth (Cole et al., 2010). Velocity was then calculated using the six point method (Stewart et al., 2001) and discretised into 10 mm by 10 mm by 10°voxels. The four orthogonal slices further from the baffles of the tank were aggregated using the symmetry of the tank to increase the data per voxel. Finally, the whole temporal data set (over 2 h of experiment) were aggregated into Eulerian plots, as described in Mesa et al. (2021),Cole et al. (2022b) and in Fig. 5.

3. Results

3.1. Tracer pathlines and occupancy

The occupancy of a tracer can be represented with different variables, as described in Cole et al. (2022a). The two most commonly used variables to represent occupancy are residence time and passes, where residence time corresponds to the time the tracer spent on each voxel, while passes are the number of times the tracer passed through a voxel (relative to entering and exiting).

Fig. 6a shows the residence time and the average tracer pathlines observed for the different tracers. The velocity field is described by pathlines instead of streamlines as the portion of the tank represented here is not a closed system. Froth overflows and is fed back into the tank, thus tracer overflow generates open

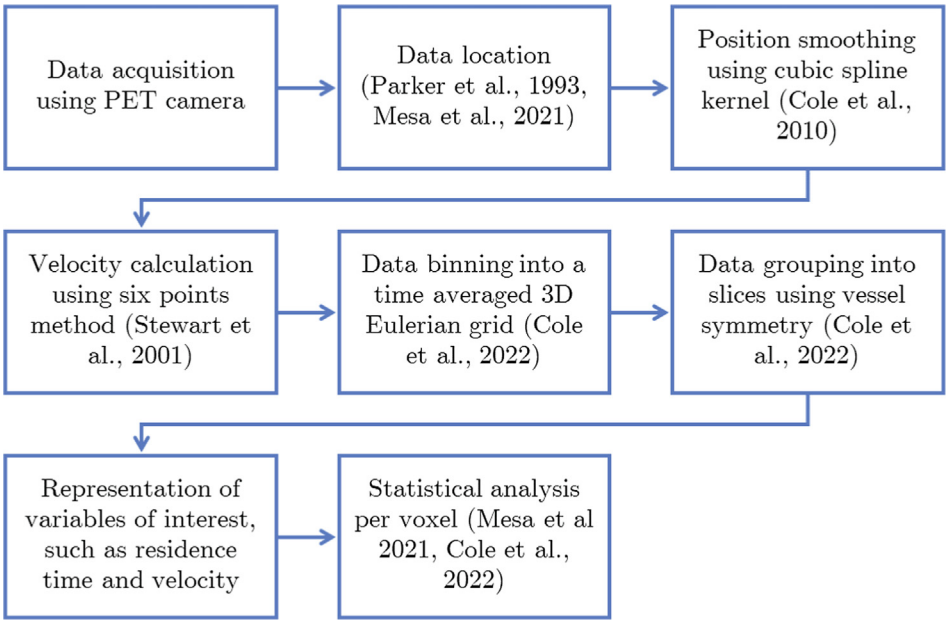

Fig. 4. Schematic flowchart detailing the PEPT data analysis procedure.

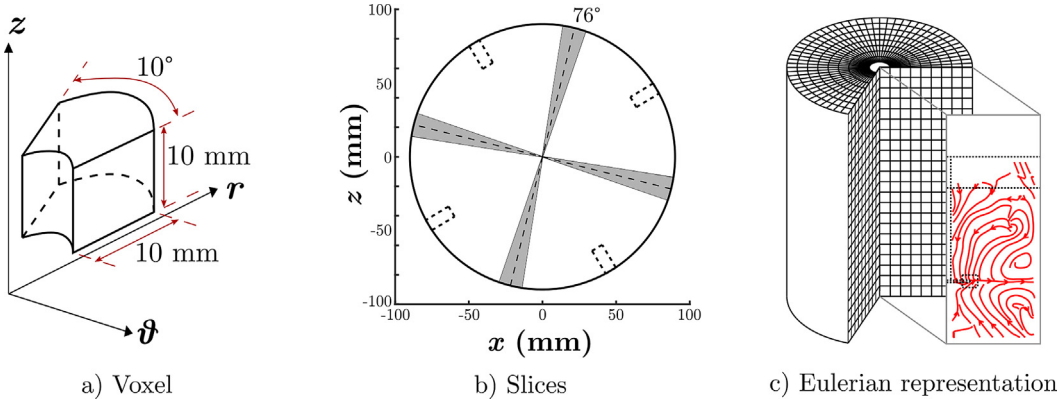

Fig. 5. Schematics showing (a) the voxel dimensions, (b) four slice angles comprising an azimuthal slice, and (c) Eulerian representation of the average particle pathlines from the PEPT data.

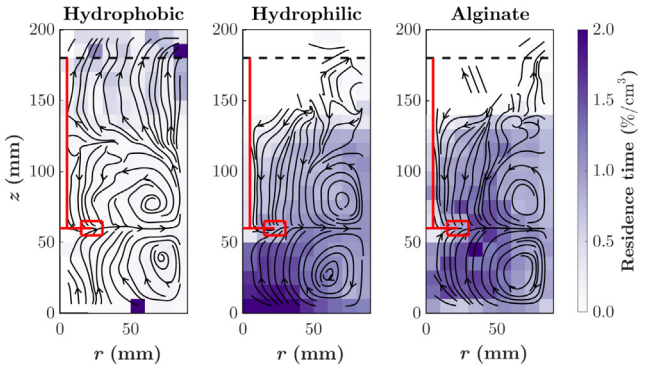

(a) Residence time per voxel, as a percentage of the total residence time in the slice, normalised by the voxel volume.

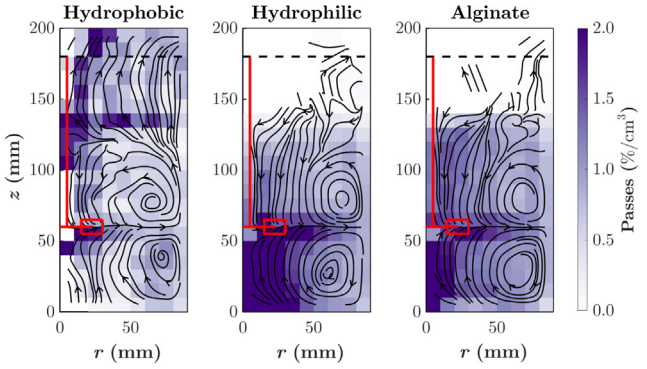

(b) Passes through each voxel as a percentage of the total passes in the slice, normalised by the volume of each voxel.

Fig. 6. Occupancy in terms of (a) Residence time and (b) Passes, for the different tracers. The Rushton turbine is detailed with red lines. The pathlines, based on the vertical and radial velocities, are shown as black arrows.

pathlines. In terms of the pathlines, all the tracers evidenced the radial flow behaviour of the Rushton impeller, characterised by the two mixing loops. Radial impellers expel fluid radially, generating an inflow towards the impeller in the vertical direction. The results clearly show that the hydrophobic and hydrophilic tracers have different flow patterns, especially in the froth zone where the hydrophobic tracer is collected into the froth, showing an upwards movement towards the top of the cell. The hydrogel tracer shows a similar flow profile to that of the hydrophilic tracer. These results suggest that the hydrophilic particles move in a similar pattern to the bulk of the liquid phase.

The residence time results clearly show that the hydrophobic tracer spends most of the time near the froth, except for one voxel near the air inlet, which could imply that the tracer anchored itself to the air-injection mesh for a period of time. Interestingly, there are differences in the residence time of the hydrophilic and hydrogel tracers. The hydrogel tracer is neutrally buoyant, which can be appreciated in the evenly distributed residence time, while the hydrophilic tracer tended to spend more time near the bottom of the cell, under the impeller. Moreover, the hydrogel tracer shows slightly lower residence times near the walls of the tank than the hydrophilic tracer.

The occupancy in terms of passes is shown in Fig. 6b. Occupancy as described in terms of the number of passes per region of interest, although less commonly used than the residence time, visualises the frequency of paths of the tracer, and it is unbiased to tracer velocity, tracer decay and non-representative events of the flow behaviour, such as the tracer becoming mechanically trapped in parts of the tank's geometry.

The results show that the hydrophobic tracer passed more times through the pulp-froth interface, and through the centre of the froth, which can be explained by the tracer dropping back after coalescence events and becoming re-attached to rising bubbles. The hydrophilic tracer passed more times through the voxels directly under the impeller and near the bottom of the cell, as well as through the discharge of the impeller. The hydrogel tracer showed similar behaviour in terms of the number of passes as that of the hydrophilic tracer, but less markedly biased towards the bottom of the tank, with some regions of high passes in the upper loop of the pulp, close the impeller shaft.

As observed in Fig. 6 a and b, the occupancy of the hydrophobic tracer is markedly different from the other tracers. The relative change in the residence time and passes from the hydrophilic to the hydrogel tracers are detailed in Fig. 7.

Notably, the hydrogel tracer results in twice the occupancy values near the pulp-froth interface relative to the hydrophilic tracer. It has been suggested that the occupancy of a tracer in PEPT can also be understood as a proxy for the concentration of the represented phase (Forster et al., 2000; Windows-Yule et al., 2020), which would imply that liquid fraction is relatively higher near the pulp-froth interface and near the wall of the tank, as shown in Fig. 7b. These observations are in agreement with predictions from computational fluid dynamics (CFD) simulations, which describe that the liquid content near the walls of a flotation tank tends to be higher, especially at the froth (Brito-Parada and Cilliers, 2012; Brito-Parada et al., 2012; Neethling et al., 2000).

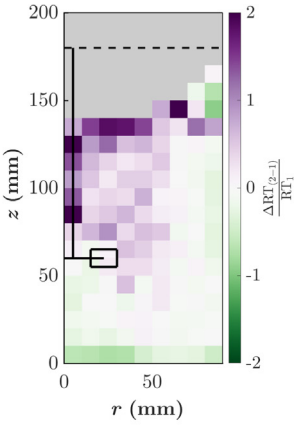

(a) Relative change of residence time, $\frac{\Delta RT_{(2-1)}}{\Delta RT_1}$

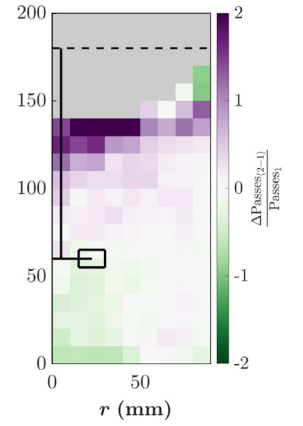

(b) Relative change in the number of passes, $\frac{\Delta Passes_{(2-1)}}{\Delta Passes_1}$

Fig. 7. Relative change in (a) residence time and (b) passes, between the hydrophilic (1) and the hydrogel (2) tracers.

3.2. Tracer velocity distributions

The velocity of the different tracers were averaged for each voxel by considering the peak of the distributions of each velocity component, the vertical ($\overline{v}_z$), radial ($\overline{v}_r$), for the different tracers, are shown in Fig. 8 as Eulerian plots of the flow. In general terms, the hydrophilic and hydrogel tracers have considerably similar distributions of the velocity components, especially for the vertical component.

The hydrophobic tracer shows a slow but clearly ascending flow in the pulp-froth interface and froth zones, implying that attachment is taking place. Notably, the hydrogel tracer presents slightly slower radial velocities than the other tracers, specially near the impeller tip and discharge.

Figs. 9 and 10 show the changing profile of the distributions of vertical and radial velocity with difference voxels across the radius of the vessel, respectively, for the different tracers at specific heights of the tank. In particular, these figures represent the velocities at the impeller discharge ($50 \leqslant z\,(\text{mm}) \leqslant 60$) and the lower end of froth ($140 \leqslant z\,(\text{mm}) \leqslant 150$).

The results show that the hydrogel tracer presents a lower upwards vertical velocity and radially outwards velocity at the discharge of the impeller compared to the other resin tracers, which behave similarly, regardless of their coating. This could relate to different drag forces due to density, size and shape.

On the other hand, near the interface the hydrophobic tracer presents slow but clearly ascending velocities. The hydrophilic and hydrogel tracers tend to present slow descending flows, specially near the walls. It can be observed that the hydrogel tracer, however, presents vertical velocity distributions with a peak near zero, with longer tails in positive velocities, implying that it has a higher tendency to move into the froth than the hydrophilic tracer.

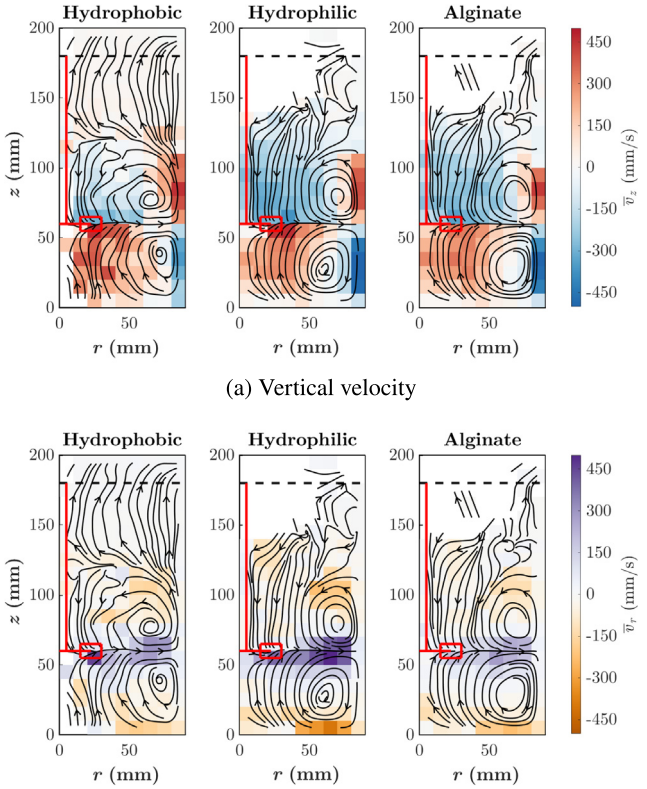

(a) Vertical velocity

(b) Radial velocity

Fig. 8. (a) Vertical and (b) radial velocity distributions of the different tracers. The Rushton turbine is detailed with red lines. The pathlines, based on the vertical and radial velocities, are shown as black arrows.

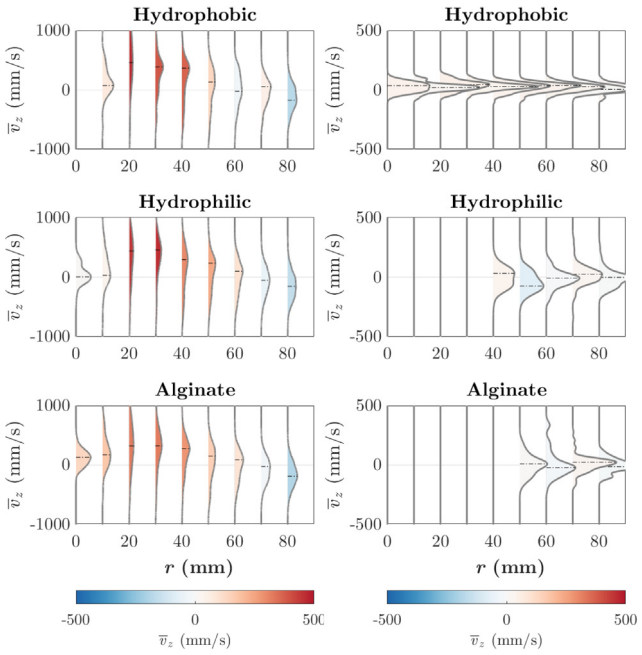

(a) Impeller discharge level ($50 \leq z\,(\text{mm}) \leq 60$)

(b) Pulp-froth interface region ($140 \leq z\,(\text{mm}) \leq 150$)

Fig. 9. Vertical velocity $\overline{v}_z$ distributions for the different tracers in voxels at different radial positions in the vessel, corresponding to (a) the level of the impeller discharge and (b) the region near the pulp-froth interface. The colour of the distribution represents the peak of the velocity distribution. Note that the y-axis scale between subfigures (a) and (b) are different, so that the features can be clearly observed.

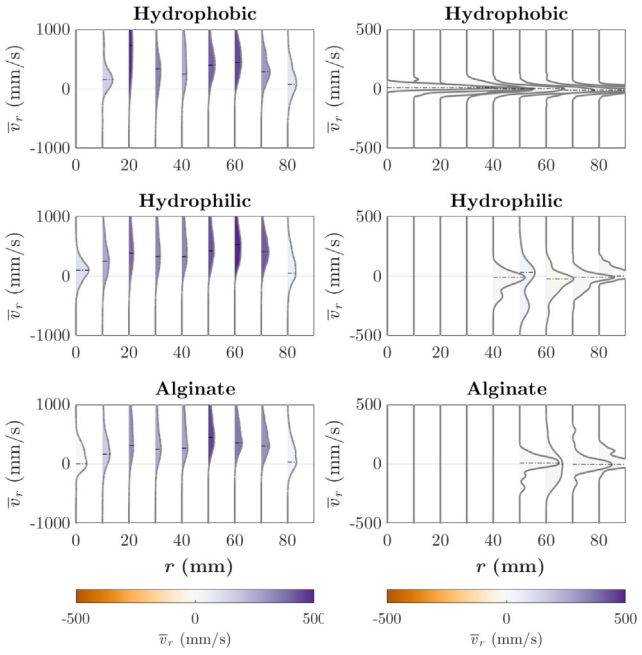

(a) Impeller discharge ($50 \leq z\,(\text{mm}) \leq 60$)

(b) Pulp-froth interface region ($140 \leq z\,(\text{mm}) \leq 150$)

Fig. 10. Radial velocity $\overline{v}_r$ distributions for the different tracers in voxels at different radial positions in the vessel, corresponding to (a) the level of the impeller discharge and (b) the region near the pulp-froth interface.The colour of the distribution represents the peak of the velocity distribution. Note that the y-axis scale between subfigures (a) and (b) are different, so that the features can be clearly observed.

In order to better visualise the previous results, Fig. 11 shows an analysis of the vertical velocity distributions for the different tracers near the wall of the tank in voxels of increasing vertical position in the vessel for a constant radial position ($80 \leqslant r\,(\text{mm}) \leqslant 90$). Results show that the hydrogel tracer is slightly more prone to overflow, with slow ascending flows in the froth zone, whilst the hydrophilic presents mainly descending flows in this zone. This is consistent with the experimental observations, as indicated by a Geiger counter at the overflow.

A comparison of the average speed distribution of the hydrogel and hydrophilic tracers are shown in Fig. 12 in terms of (a) the absolute difference in speed, (b) relative change in speed and (c) Jensen-Shannon (J-S) distance of the difference in speed. The use of the relative change allows to eliminate the bias of the different orders of magnitude of the tracer speed in the pulp ($\sim$ 1 m/s) and the froth ($\sim$ 1 cm/s). The J-S distance, calculated as the square root of the J-S divergence, is a non-parametric statistical test of differences between two distributions, where 0 represents identical distributions and 1 is for completely different distributions. The J-S distance has been used previously with PEPT data to highlight important differences in flow properties of impeller designs (more details are provided in Mesa et al., 2021).

The results in Fig. 12a show that the hydrogel tracer generally moves slower than the hydrophilic tracer, especially near the impeller discharge. However, the Jensen-Shannon distance indicates that the main difference in speed occurs at the pulp-froth interface near the wall (Fig. 12c), where the hydrogel tracer moves considerably faster in relative terms, as shown in Fig. 12b.

Fig. 13 shows the differences in vertical velocity between the hydrophilic and hydrogel tracers in vectorial terms for each voxel, represented as $\Delta\overline{v}_{z_{(2-1)}}$. The comparison is shown in terms of (a) absolute vectorial difference, (b) relative difference, and (c) the Jensen-Shannon distance of the vertical velocity distributions. Since $\Delta\overline{v}_{z_{(2-1)}}$ is a vectorial difference, it implies that the resulting sign for each voxel represents the relative sense of motion, *i.e.*, positive if the hydrogel tracer moves upwards faster, or downwards slower, than the hydrophilic tracer. It can be observed in Fig. 13a that the hydrogel has an overall tendency to move upwards relative to the hydrophilic tracer, which could be related to it being neutrally-buoyant. This tendency is markedly higher near the walls of the tank, where the hydrogel tracer presents up to three times faster ascending flows in relative terms, as shown in Fig. 13b. The Jensen-Shannon distance (Fig. 13c), however, shows that the most important difference in terms of the vertical velocity distribution occurs at the pulp-froth interface, specially near the wall and near the shaft.

Assuming that the hydrogel tracer is following the liquid flow, these experimental results suggest that liquid in the flotation

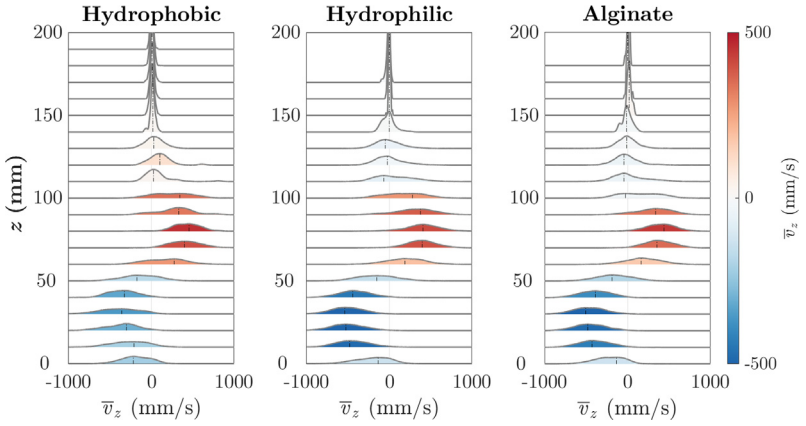

Fig. 11. Vertical velocity distributions of the three tracer particles in voxels with increasing vertical position, near the wall of the tank corresponding to a radial position ($80 \leqslant r\,(\text{mm}) \leqslant 90$).

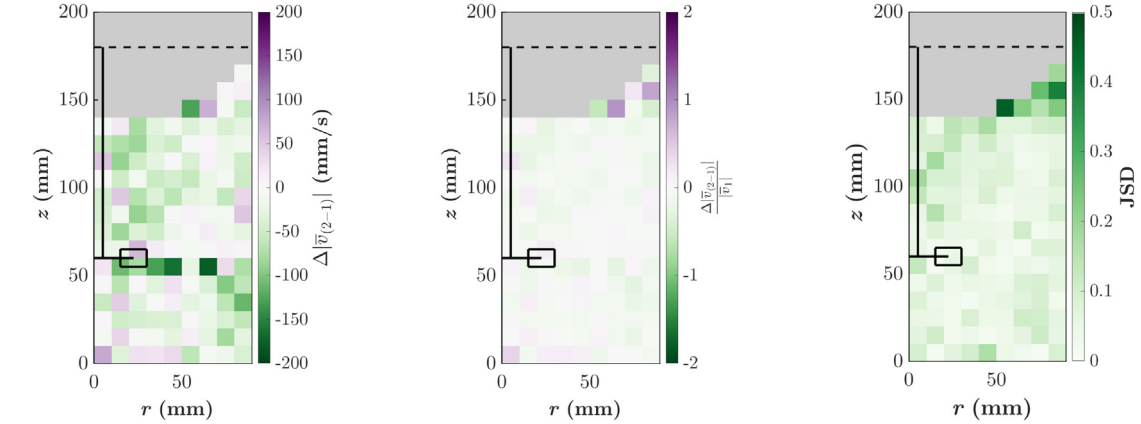

(a) Speed difference, $\Delta|\overline{v}_{(2-1)}|$ (mm/s) (b) Speed relative change, $\frac{\Delta|\overline{v}_{(2-1)}|}{|\overline{v}_1|}$ (c) Jensen-Shannon distance

Fig. 12. Representations of differences in the speed distributions between the hydrophilic (1) and the hydrogel (2) tracers, in terms of (a) absolute speed difference, (b) relative change in speed and (c) the Jensen-Shannon distance of the speed distributions.

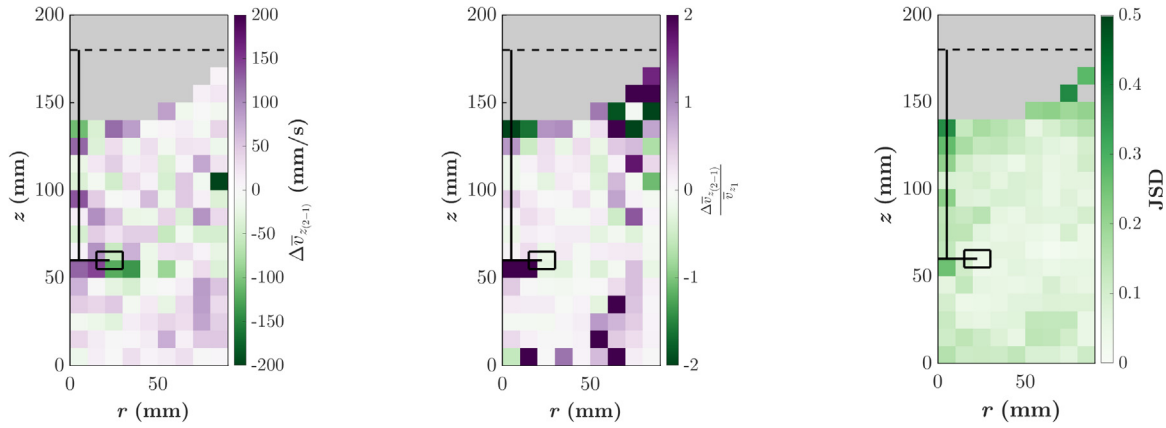

(a) Vertical velocity difference, $\Delta\overline{v}_{z_{(2-1)}}$ (mm/s) (b) Vertical velocity relative change, $\frac{\Delta\overline{v}_{z_{(2-1)}}}{|\overline{v}_{z_1}|}$ (c) Jensen-Shannon distance

Fig. 13. Representations of differences in the vertical velocity distributions between the hydrophilic (1) and the hydrogel (2) tracers, in terms of (a) absolute speed difference, (b) relative change in speed and (c) the Jensen-Shannon distance of the speed distributions.

vessel tends to ascend faster near the walls, especially at the froth and pulp-froth interface. These observations are also in agreement with previous CFD predictions for flotation, which had been validated with water-only experiments (Schwarz et al., 2019; Yan et al., 2021).

4. Conclusions

In this work, a new neutrally-buoyant hydrogel tracer fabricated from alginate methods, capable of withstanding the high turbulence of a flotation cell, has been used for PEPT measurements. Comparison between the hydrogel tracer and two resin tracers with different coatings to change their specific surface properties - namely, a hydrophilic and a hydrophobic tracer - show that the hydrogel tracer presents similar flow patterns and velocity distributions to the hydrophilic tracer. The motion of the hydrophobic tracer is different to both the hydrophilic and hydrogel tracers. Nevertheless, a series of statistical analyses, including the Jensen-Shannon distance between the velocity distributions for each voxel, show that the hydrogel and hydrophilic tracer have different velocity distributions, especially near the walls and close to the froth zone. Notably, fast ascending flows are described near the walls of the tank for the hydrogel tracer, which implies the presence of fast ascending water flows, a phenomena that had been described before in computational fluid dynamics models, but had not been quantified in three-phase experimental systems before. Future research should consider the potential for even smaller tracers to further study the hydrodynamics of small turbulent eddies, as well as the laminar flows within the Plateau borders in the froth.

CRediT authorship contribution statement

Diego Mesa: Methodology, Software, Formal analysis, Investigation, Data Curation, Writing - Original Draft, Visualisation, Funding acquisition. **Michael van Heerden:** Conceptualisation, Methodology, Investigation, Data Curation. **Katie E. Cole:** Conceptualisation, Methodology, Software, Formal analysis, Resources, Data Curation, Writing - Review & Editing, Visualisation. **Stephen J. Neethling:** Resources, Project administration, Funding acquisition. **Pablo R. Brito-Parada:** Conceptualisation, Resources, Investigation, Writing - Review & Editing, Supervision, Project administration, Funding acquisition.

Declaration of Competing Interest

The authors declare that they have no known competing financial interests or personal relationships that could have appeared to influence the work reported in this paper.

Acknowledgements

The authors acknowledge funding from the European Union's Horizon 2020 research and innovation programme FineFuture under grant agreement No. 821265. D. Mesa also acknowledges the financial support of the Institute of Materials, Minerals and Mining (IOM3).

References

Al-Shemmeri, M., Windows-Yule, K., Lopez-Quiroga, E., Fryer, P.J., 2021. Coffee bean particle motion in a spouted bed measured using Positron Emission Particle Tracking (PEPT). J. Food Eng. 311, 110709. https://doi.org/10.1016/j.jfoodeng.2021.110709.

Alves, S.S., Maia, C.I., Vasconcelos, J.M.T., Serralheiro, A.J., 2002. Bubble size in aerated stirred tanks. Chem. Eng. J. 89, 109–117. https://doi.org/10.1016/S1385-8947(02)00008-6.

Armenante, P.M., Luo, C., Chou, C.C., Fort, I., Medek, J., 1997. Velocity profiles in a closed, unbaffled vessel: comparison between experimental LDV data and numerical CFD predictions. Chem. Eng. Sci. 52, 3483–3492. https://doi.org/10.1016/S0009-2509(97)00150-4.

Ascanio, G., 2015. Mixing time in stirred vessels: A review of experimental techniques. Chin. J. Chem. Eng. 23, 1065–1076. https://doi.org/10.1016/j.cjche.2014.10.022.

Bakalis, S., Fryer, P.J., Parker, D.J., 2004. Measuring velocity distributions of viscous fluids using positron emission particle tracking (PEPT). AIChE Journal 50, 1606–1613. doi: 10.1002/aic.10153, URL: https://aiche.onlinelibrary.wiley.com/doi/abs/10.1002/aic.10153, arXiv:https://aiche.onlinelibrary.wiley.com/doi/pdf/10.1002/aic.10153.

Boden, S., Bieberle, M., Hampel, U., 2008. Quantitative measurement of gas hold-up distribution in a stirred chemical reactor using X-ray cone-beam computed tomography. Chem. Eng. J. 139, 351–362. https://doi.org/10.1016/j.cej.2007.08.014. URL: https://www.sciencedirect.com/science/article/pii/S1385894707005736.

Boucher, D., Jordens, A., Sovechles, J.M., Langlois, R., Leadbeater, T.W., Rowson, N.A., Cilliers, J.J., Waters, K.E., 2017. Direct mineral tracer activation in positron emission particle tracking of a flotation cell. Miner. Eng. 100, 155–165. https://doi.org/10.1016/j.mineng.2016.10.022.

Brady, M.R., Telionis, D.P., Vlachos, P.P., Yoon, R.H., 2006. Evaluation of multiphase flotation models in grid turbulence via Particle Image Velocimetry. Int. J. Miner. Process. 80, 133–143. https://doi.org/10.1016/j.minpro.2006.03.010.

Brito-Parada, P.R., Cilliers, J.J., 2012. Experimental and numerical studies of launder configurations in a two-phase flotation system. Miner. Eng. 36–38, 119–125. https://doi.org/10.1016/j.mineng.2012.03.009.

Brito-Parada, P.R., Neethling, S.J., Cilliers, J.J., 2012. CFD study of liquid drainage in flotation foams. In: Lockhart Bogle, I.D., Fairweather, M. (Eds.), 22nd European Symposium on Computer Aided Process Engineering. Elsevier B.V, London, UK, pp. 1143–1147. https://doi.org/10.1016/B978-0-444-59520-1.50087-7.

Buffler, A., Cole, K.E., Leadbeater, T.W., van Heerden, M.R., 2018. Positron emission particle tracking: A powerful technique for flow studies. Int. J. Modern Phys.: Conf. Ser. 48, 1860113. https://doi.org/10.1142/S2010194518601138.

Chiti, F., Bakalis, S., Bujalski, W., Barigou, M., Eaglesham, A., Nienow, A.W., 2011. Using positron emission particle tracking (PEPT) to study the turbulent flow in a baffled vessel agitated by a Rushton turbine: Improving data treatment and validation. Chem. Eng. Res. Des. 89, 1947–1960. https://doi.org/10.1016/j.cherd.2011.01.015. URL: https://www.sciencedirect.com/science/article/pii/S0263876211000414.

Cole, K.E., Barker, D.J., Brito-Parada, P.R., Buffler, A., Hadler, K., Mackay, I., Mesa, D., Morrison, A.J., Neethling, S., Norori-McCormac, A., Shean, B., Cilliers, J., 2022a. Standard method for performing positron emission particle tracking (PEPT) measurements of froth flotation at PEPT Cape Town. MethodsX. https://doi.org/10.1016/j.mex.2022.101680.

Cole, K.E., Brito-Parada, P.R., Hadler, K., Mesa, D., Neethling, S.J., Norori-McCormac, A.M., Cilliers, J.J., 2022b. Characterisation of solid hydrodynamics in a three-phase stirred tank reactor with positron emission particle tracking (PEPT). Chem. Eng. J., 133819 https://doi.org/10.1016/j.cej.2021.133819.

Cole, K.E., Buffler, A., Cilliers, J.J., Govender, I., Heng, J.Y., Liu, C., Parker, D.J., Shah, U. V., van Heerden, M.R., Fan, X., 2014. A surface coating method to modify tracers for positron emission particle tracking (PEPT) measurements of froth flotation. Powder Technol. 263, 26–30. https://doi.org/10.1016/j.powtec.2014.04.083.

Cole, K.E., Waters, K.E., Parker, D.J., Neethling, S.J., Cilliers, J.J., 2010. PEPT combined with high speed digital imaging for particle tracking in dynamic foams. Chem. Eng. Sci. 65, 1887–1890. https://doi.org/10.1016/j.ces.2009.10.010.

de Lamotte, A., Delafosse, A., Calvo, S., Delvigne, F., Toye, D., 2017. Investigating the effects of hydrodynamics and mixing on mass transfer through the free-surface in stirred tank bioreactors. Chem. Eng. Sci. 172, 125–142. https://doi.org/10.1016/j.ces.2017.06.028.

de Lamotte, A., Delafosse, A., Calvo, S., Toye, D., 2018. Analysis of PIV measurements using modal decomposition techniques, POD and DMD, to study flow structures and their dynamics within a stirred-tank reactor. Chem. Eng. Sci. 178, 348–366. https://doi.org/10.1016/j.ces.2017.12.047.

Deglon, D.A., 2005. The effect of agitation on the flotation of platinum ores. Miner. Eng. 18, 839–844. https://doi.org/10.1016/j.mineng.2005.01.024.

Eckert, R.E., McLaughlin, C.M., Rushton, J.H., 1985. Liquid-liquid interfacial areas formed by turbine impellers in baffled, cylindrical mixing tanks. AIChE J. 31, 1811–1820. https://doi.org/10.1002/aic.690311107.

Fairhurst, P.G., Barigou, M., Fryer, P.J., Pain, J.P., Parker, D.J., 2001. Using positron emission particle tracking (PEPT) to study nearly neutrally buoyant particles in high solid fraction pipe flow. Int. J. Multiph. Flow 27, 1881–1901. https://doi.org/10.1016/S0301-9322(01)00038-6.

Fan, X., Parker, D., Smith, M., 2006. Enhancing 18f uptake in a single particle for positron emission particle tracking through modification of solid surface chemistry. Nucl. Instrum. Methods Phys. Res., Sect. A 558, 542–546. https://doi.org/10.1016/j.nima.2005.12.186.

Fan, X., Parker, D.J., Smith, M.D., 2006. Labelling a single particle for positron emission particle tracking using direct activation and ion-exchange techniques. Nucl. Instrum. Methods Phys. Res., Sect. A 562, 345–350. https://doi.org/10.1016/j.nima.2006.03.015.

Fangary, Y., Barigou, M., Seville, J., Parker, D., 2000. Fluid trajectories in a stirred vessel of non-newtonian liquid using positron emission particle tracking. Chem. Eng. Sci. 55, 5969–5979. https://doi.org/10.1016/S0009-2509(00)00176-7. URL: https://www.sciencedirect.com/science/article/pii/S0009250900001767.

Ford, J.J., Heindel, T.J., Jensen, T.C., Drake, J.B., 2008. X-ray computed tomography of a gas-sparged stirred-tank reactor. Chem. Eng. Sci. 63, 2075–2085. https://doi.org/10.1016/j.ces.2008.01.007. URL: https://www.sciencedirect.com/science/article/pii/S0009250908000079.

Forster, R., Seville, J., Parker, D., Ding, Y., 2000. Tracking Single Particles in Process Equipment or Probing Processes Using Positrons. KONA Powder and Particle Journal 18, 139–148. doi:10.14356/kona.2000020.

Gomez, C.O., Finch, J.A., 2007. Gas dispersion measurements in flotation cells. Int. J. Miner. Process. 84, 51–58. https://doi.org/10.1016/j.minpro.2007.03.009.

Grau, R., Heiskanen, K., 2002. Visual technique for measuring bubble size in flotation machines. Miner. Eng. 15, 507–513. https://doi.org/10.1016/S0892-6875(02)00074-2.

Hampel, U., Hristov, H.V., Bieberle, A., Zippe, C., 2007. Application of high-resolution gamma ray tomography to the measurement of gas hold-up distributions in a stirred chemical reactor. Flow Meas. Instrum. 18, 184–190. https://doi.org/10.1016/j.flowmeasinst.2007.06.001. URL: https://www.sciencedirect.com/science/article/pii/S0955598607000374.

Hashemi, N., Ein-Mozaffari, F., Upreti, S.R., Hwang, D.K., 2016. Analysis of mixing in an aerated reactor equipped with the coaxial mixer through electrical resistance tomography and response surface method. Chem. Eng. Res. Des. 109, 734–752. https://doi.org/10.1016/j.cherd.2016.03.028. URL: https://www.sciencedirect.com/science/article/pii/S0263876216300338.

Kumaresan, T., Joshi, J.B., 2006. Effect of impeller design on the flow pattern and mixing in stirred tanks. Chem. Eng. J. 115, 173–193. https://doi.org/10.1016/j.cej.2005.10.002.

Laamanen, C.A., Ross, G.M., Scott, J.A., 2016. Flotation harvesting of microalgae. Renew. Sustain. Energy Rev. 58, 75–86. https://doi.org/10.1016/j.rser.2015.12.293.

Langford, S., Wiggins, C., Tenpenny, D., Ruggles, A., 2016. Positron Emission Particle Tracking (PEPT) for Fluid Flow Measurements. Nucl. Eng. Des. 302, 81–89. https://doi.org/10.1016/j.nucengdes.2016.01.017. URL: https://www.sciencedirect.com/science/article/pii/S0029549316000273.

Liu, J., Wang, H., Hu, T., Bai, X., Wang, S., Xie, W., Hao, J., He, Y., 2020. Recovery of LiCoO2 and graphite from spent lithium-ion batteries by cryogenic grinding and froth flotation. Miner. Eng. 148, 106223. https://doi.org/10.1016/j.mineng.2020.106223.

Liu, Y.J., Li, W., Han, L.C., Cao, Y., Luo, H.a., Al-Dahhan, M., Dudukovic, M.P., 2011. -CT measurement and CFD simulation of cross section gas holdup distribution in a gas–liquid stirred standard Rushton tank. Chemical Engineering Science 66, 3721–3731. doi:10.1016/j.ces.2011.03.042.

Mackay, I., Videla, A.R., Brito-Parada, P.R., 2020. The link between particle size and froth stability - Implications for reprocessing of flotation tailings. J. Clean. Prod. 242, 118436. https://doi.org/10.1016/j.jclepro.2019.118436.

Martín, M., Montes, F.J., Galán, M.A., 2008. Bubbling process in stirred tank reactors I: Agitator effect on bubble size, formation and rising. Chem. Eng. Sci. 63, 3212–3222. https://doi.org/10.1016/j.ces.2008.03.028.

Mavros, P., 2001. Flow Visualization in Stirred Vessels: A Review of Experimental Techniques. Chem. Eng. Res. Des. 79, 113–127. https://doi.org/10.1205/02638760151095926.

Mavros, P., Xuereb, C., Fort, I., Bertrand, J., 2002. Investigation by laser Doppler velocimetry of the effects of liquid flow rates and feed positions on the flow patterns induced in a stirred tank by an axial-flow impeller. Chem. Eng. Sci. 57, 3939–3952. https://doi.org/10.1016/S0009-2509(02)00268-3.

Maximiano Raimundo, P., Cloupet, A., Cartellier, A., Beneventi, D., Augier, F., 2019. Hydrodynamics and scale-up of bubble columns in the heterogeneous regime: Comparison of bubble size, gas holdup and liquid velocity measured in 4 bubble columns from 0.15m to 3m in diameter. Chem. Eng. Sci. 198, 52–61. https://doi.org/10.1016/j.ces.2018.12.043.

Mesa, D., Brito-Parada, P.R., 2019. Scale-up in froth flotation: A state-of-the-art review. Sep. Purif. Technol. 210, 950–962. https://doi.org/10.1016/j.seppur.2018.08.076.

Mesa, D., Brito-Parada, P.R., 2020. Bubble size distribution in aerated stirred tanks: Quantifying the effect of stator-impeller design. Chem. Eng. Res. Des. 160, 356–369. https://doi.org/10.1016/j.cherd.2020.05.029.

Mesa, D., E., K.C., van Heerden, M.R., Brito-Parada, P.R., 2021. Hydrodynamic characterisation of flotation impeller designs using Positron Emission Particle Tracking (PEPT). Separation and Purification Technology 276, 119316. doi:10.1016/j.seppur.2021.119316.

Mesa, D., Morrison, A.J., Brito-Parada, P.R., 2020. The effect of impeller-stator design on bubble size: implications for froth stability and flotation performance. Miner. Eng. 157, 106533. https://doi.org/10.1016/j.mineng.2020.106533.

Montante, G., Horn, D., Paglianti, A., 2008. Gas-liquid flow and bubble size distribution in stirred tanks. Chem. Eng. Sci. 63, 2107–2118. https://doi.org/10.1016/j.ces.2008.01.005.

Montante, G., Paglianti, A., 2015. Gas hold-up distribution and mixing time in gas–liquid stirred tanks. Chem. Eng. J. 279, 648–658. https://doi.org/10.1016/j.cej.2015.05.058.

Neethling, S.J., Cilliers, J.J., Woodburn, E.T., 2000. Prediction of the water distribution in a flowing foam. Chem. Eng. Sci. 55, 4021–4028. https://doi.org/10.1016/S0009-2509(00)00054-3.

Negari, M.S., Ostad Movahed, S., Ahmadpour, A., 2018. Separation of polyvinylchloride (PVC), polystyrene (PS) and polyethylene terephthalate (PET) granules using various chemical agents by flotation technique. Sep. Purif. Technol. 194, 368–376. https://doi.org/10.1016/j.seppur.2017.11.062.

Norori-McCormac, A., Brito-Parada, P.R., Hadler, K., Cole, K.E., Cilliers, J.J., 2017. The effect of particle size distribution on froth stability in flotation. Sep. Purif. Technol. 184, 240–247. https://doi.org/10.1016/j.seppur.2017.04.022.

Parker, D.J., Broadbent, C.J., Fowles, P., Hawkesworth, M.R., McNeil, P., 1993. Positron emission particle tracking - a technique for studying flow within engineering equipment. Nucl. Instrum. Methods Phys. Res., Sect. A 326, 592–607. https://doi.org/10.1016/0168-9002(93)90864-E.

Pérez-Mohedano, R., Letzelter, N., Amador, C., van der Roest, C.T., Bakalis, S., 2015. Positron Emission Particle Tracking (PEPT) for the analysis of water motion in a domestic dishwasher. Chem. Eng. J. 259, 724–736. https://doi.org/10.1016/j.cej.2014.08.033.

Pianko-Oprych, P., Nienow, A., Barigou, M., 2009. Positron emission particle tracking (PEPT) compared to particle image velocimetry (PIV) for studying the flow generated by a pitched-blade turbine in single phase and multi-phase systems. Chem. Eng. Sci. 64, 4955–4968. https://doi.org/10.1016/j.ces.2009.08.003.

Polat, H., Erdogan, D., 2007. Heavy metal removal from waste waters by ion flotation. J. Hazard. Mater. 148, 267–273. https://doi.org/10.1016/j.jhazmat.2007.02.013.

Rao, F., Liu, Q., 2013. Froth Treatment in Athabasca Oil Sands Bitumen Recovery Process: A Review. Energy & Fuels 27, 7199–7207. https://doi.org/10.1021/ef4016697.

Rosseburg, A., Fitschen, J., Wutz, J., Wucherpfennig, T., Schlüter, M., 2018. Hydrodynamic inhomogeneities in large scale stirred tanks – Influence on mixing time. Chem. Eng. Sci. 188, 208–220. https://doi.org/10.1016/j.ces.2018.05.008.

Ruismäki, R., Rinne, T., Danczak, A., Taskinen, P., Serna-Guerrero, R., Jokilaakso, A., 2020. Integrating Flotation and Pyrometallurgy for Recovering Graphite and Valuable Metals from Battery Scrap. Metals 10, 680. https://doi.org/10.3390/met10050680. number: 5 Publisher: Multidisciplinary Digital Publishing Institute.

Rushton, J.H., Costich, E.W., Everett, H.J., 1950. Power characteristics of mixing impellers, Parts 1 and 2. Chem. Eng. Prog.

Saththasivam, J., Loganathan, K., Sarp, S., 2016. An overview of oil-water separation using gas flotation systems. Chemosphere 144, 671–680. https://doi.org/10.1016/j.chemosphere.2015.08.087.

Schubert, H., 2008. On the optimization of hydrodynamics in fine particle flotation. Miner. Eng. 21, 930–936. https://doi.org/10.1016/j.mineng.2008.02.012.

Schwarz, M.P., Koh, P.T.L., Wu, J., Nguyen, B., Zhu, Y., 2019. Modelling and measurement of multi-phase hydrodynamics in the Outotec flotation cell. Miner. Eng. 144, 106033. https://doi.org/10.1016/j.mineng.2019.106033.

Sommer, A.E., Rox, H., Shi, P., Eckert, K., Rzehak, R., 2021. Solid-liquid flow in stirred tanks: "CFD-grade experimental investigation. Chem. Eng. Sci. 245, 116743. https://doi.org/10.1016/j.ces.2021.116743.

Spinks, T.J., Jones, T., Bloomfield, P.M., Bailey, D.L., Miller, M., Hogg, D., Jones, W.F., Vaigneur, K., Reed, J., Young, J., Newport, D., Moyers, C., Casey, M.E., Nutt, R., 2000. Physical characteristics of the ECAT EXACT3D positron tomograph. Physics in Medicine and Biology 45, 2601–2618. https://doi.org/10.1088/0031-9155/45/9/313, publisher: IOP Publishing.

Stewart, R.L., Bridgwater, J., Zhou, Y.C., Yu, A.B., 2001. Simulated and measured flow of granules in a bladed mixer–a detailed comparison. Chem. Eng. Sci. 56, 5457–5471. https://doi.org/10.1016/S0009-2509(01)00190-7.

Tabosa, E., Runge, K., Holtham, P., 2016. The effect of cell hydrodynamics on flotation performance. Int. J. Miner. Process. 156, 99–107. https://doi.org/10.1016/j.minpro.2016.05.019.

van Heerden, M.R., Cole, K.E., van der Meulen, N., Franzidis, J., Buffler, A., 2020. Extending the life of SnO2 68Ge/68Ga generators used in the radiolabelling of ion exchange resins. Appl. Radiat. Isot. 158, 109044. https://doi.org/10.1016/j.apradiso.2020.109044.

van Heerden, M.R., Perin, R., Cole, K.E., Buffler, A., Leadbeater, T., Peterson, S., Shock, J., Mesa, D., Brito-Parada, P., 2022. Development of hydrogel tracer particles for positron emission particle tracking (PEPT) measurements of multiphase flows. Submitted to MethodsX.

Vashisth, S., Bennington, C.P., Grace, J.R., Kerekes, R.J., 2011. Column Flotation Deinking: State-of-the-art and opportunities. Resour. Conserv. Recycl. 55, 1154–1177. https://doi.org/10.1016/j.resconrec.2011.06.013.

Wang, C.Q., Wang, H., Fu, J.G., Liu, Y.N., 2015. Flotation separation of waste plastics for recycling–A review. Waste Manage. 41, 28–38. https://doi.org/10.1016/j.wasman.2015.03.027.

Wang, M., Dorward, A., Vlaev, D., Mann, R., 2000. Measurements of gas–liquid mixing in a stirred vessel using electrical resistance tomography (ERT). Chem. Eng. J. 77, 93–98. https://doi.org/10.1016/S1385-8947(99)00138-2. URL: https://www.sciencedirect.com/science/article/pii/S1385894799001382.

Waters, K.E., Rowson, N., Fan, X., Parker, D., Cilliers, J.J., 2008. Positron emission particle tracking as a method to map the movement of particles in the pulp and froth phases. Miner. Eng. 21, 877–882. https://doi.org/10.1016/j.mineng.2008.02.007.

Wiggins, C., Patel, N., Bingham, Z., Ruggles, A., 2019. Qualification of multiple-particle positron emission particle tracking (M-PEPT) technique for measurements in turbulent wall-bounded flow. Chem. Eng. Sci. 204, 246–256. https://doi.org/10.1016/j.ces.2019.04.030. URL: https://www.sciencedirect.com/science/article/pii/S0009250919303951.

Wills, B.A., Finch, J.A., 2016. Froth Flotation. Elsevier. chapter 12th. pp. 265–380. doi:10.1016/B978-0-08-097053-0.00012-1.

Windows-Yule, C., Seville, J., Ingram, A., Parker, D., 2020. Positron Emission Particle Tracking of Granular Flows. Annual Review of Chemical and Biomolecular Engineering 11, 367–396. https://doi.org/10.1146/annurev-chembioeng-011620-120633.

Xiao, Y., Li, X., Ren, S., Mao, Z.S., Yang, C., 2020. Hydrodynamics of gas phase under typical industrial gassing rates in a gas-liquid stirred tank using intrusive image-based method. Chem. Eng. Sci. 227, 115923. https://doi.org/10.1016/j.ces.2020.115923. URL: https://www.sciencedirect.com/science/article/pii/S0009250920304553.

Yan, X., Yao, Y., Meng, S., Zhao, S., Wang, L., Zhang, H., Cao, Y., 2021. Comprehensive particle image velocimetry measurement and numerical model validations on the gas–liquid flow field in a lab-scale cyclonic flotation column. Chem. Eng. Res. Des. 174, 1–10. https://doi.org/10.1016/j.cherd.2021.07.024.

Yang, C., Mao, Z.S., 2014. Multiphase Stirred Reactors. Elsevier. chapter 3rd. pp. 75–151. doi:10.1016/B978-0-08-099919-7.00003-2.

Yu, J., He, Y., Ge, Z., Li, H., Xie, W., Wang, S., 2018. A promising physical method for recovery of LiCoO2 and graphite from spent lithium-ion batteries: Grinding flotation. Sep. Purif. Technol. 190, 45–52. https://doi.org/10.1016/j.seppur.2017.08.049.

Yu, S., Wu, C.Y., Adams, M.J., Reynolds, G., Gururajan, B., Gargiuli, J., Leadbeater, T., Roberts, R., Parker, D.J., 2015. The use of positron emission particle tracking (PEPT) to study milling of roll-compacted microcystalline cellulose ribbons. Powder Technol. 285, 74–79. https://doi.org/10.1016/j.powtec.2015.06.051.

Zhang, G., He, Y., Feng, Y., Wang, H., Zhu, X., 2018. Pyrolysis-Ultrasonic-Assisted Flotation Technology for Recovering Graphite and LiCoO2 from Spent Lithium-Ion Batteries. ACS Sustain. Chem. Eng. 6, 10896–10904. https://doi.org/10.1021/acssuschemeng.8b02186, publisher: American Chemical Society.